Article

On-device lead sequestration for perovskite solar cells

https://doi.org/10.1038/s41586-020-2001-x

Received: 25 June 2019

Accepted: 14 November 2019

Published online: 19 February 2020

Check for updates

Xun Li[1,5], Fei Zhang[2,5], Haiying He[1,4], Joseph J. Berry[3], Kai Zhu[2]✉ & Tao Xu[1]✉

Perovskite solar cells, as an emerging high-efficiency and low-cost photovoltaic technology[1–6], face obstacles on their way towards commercialization. Substantial improvements have been made to device stability[7–10], but potential issues with lead toxicity and leaching from devices remain relatively unexplored[11–16]. The potential for lead leakage could be perceived as an environmental and public health risk when using perovskite solar cells in building-integrated photovoltaics[17–23]. Here we present a chemical approach for on-device sequestration of more than 96 per cent of lead leakage caused by severe device damage. A coating of lead-absorbing material is applied to the front and back sides of the device stack. On the glass side of the front transparent conducting electrode, we use a transparent lead-absorbing molecular film containing phosphonic acid groups that bind strongly to lead. On the back (metal) electrode side, we place a polymer film blended with lead-chelating agents between the metal electrode and a standard photovoltaic packing film. The lead-absorbing films on both sides swell to absorb the lead, rather than dissolve, when subjected to water soaking, thus retaining structural integrity for easy collection of lead after damage.

For a typical 550-nm-thick lead (Pb)-based perovskite solar cell (PSC), the unit area concentration of Pb is estimated to be about 0.75 g m^{-2} (Methods)[13,24], which is more than 100 times higher than that of present-day Pb-containing paints (about 0.007 g m^{-2}), but an order of magnitude less than for Pb-based paints (about 10 g m^{-2}) that have long been prohibited[25,26]. Enhanced physical encapsulation can lessen Pb leakage from devices when subjected to mild environmental damage[27]. However, it is more desirable to develop strategies that avoid potential Pb leakage to the environment—whether to the air, underground water or soil. Strategies for glass encapsulation to address fire hazards have been reported[28], but yet to be addressed are water ingress to the water-vulnerable perovskite layer and the subsequent irreversible outflow of Pb into underground water and/or soils.

A schematic of our device configuration is shown in Fig. 1a. A transparent Pb-absorbing *P*,*P*′-di(2-ethylhexyl)methanediphosphonic acid (DMDP) film (Fig. 1b) is deposited on the glass. Extended Data Fig. 1 shows that DMDP coatings with thicknesses ranging from 0.7 to 6.89 μm are all highly transparent. The two phosphonic acid groups in each DMDP molecule can strongly bind with a Pb^{2+} ion (Fig. 1c), with a calculated binding energy of 295.6 kJ mol^{-1} (Extended Data Fig. 2). DMDP is soluble in certain polar organic solvents (for example, ethanol), allowing for film deposition by common solution coating methods. The DMDP film is insoluble in water, but has good water permeability. As such, the functional phosphonic acid groups can effectively absorb Pb^{2+} in water when water seeps into the device.

The Pb-absorbing capability of the DMDP films on glass substrate was first examined by soaking the films in lead iodide (PbI_2) aqueous solutions and studying the time-dependent Pb^{2+} concentration in the solutions. The Pb leakage from six pristine PSCs and the measurements from PbI_2 solutions with known concentrations were used as references to verify the accuracy of the measurements within a satisfactory range (Extended Data Fig. 3). For a typical roughly 2.36-μm-thick DMDP film used in the device (Fig. 1a), the amount of DMDP (about 6.19×10^{-7} mol DMDP cm^{-2}) is about 1.7 times greater than the amount of Pb (about 3.63×10^{-7} mol Pb^{2+} cm^{-2}) in a typical PSC, assuring adequate Pb^{2+} binding sites. Also worth noting is that the average annual rain precipitation is 77 cm in the United States[29], which corresponds to about 300 ml of water for a 4-cm^2 area. Thus, if the amount of Pb^{2+} within the 4-cm^2 device was completely dissolved by the rainwater (about 300 ml), then the Pb^{2+} concentration would be 4.84×10^{-6} M (about 1 ppm Pb^{2+}). To pre-evaluate the Pb-sequestrating effect of the 2.36-μm-thick DMDP film, we chose to worsen the condition by increasing the PbI_2 concentration to 1.93×10^{-5} M (about 4 ppm Pb^{2+}). We soaked a 4-cm^2, 2.36-μm-thick DMDP film (containing 2.48×10^{-6} mol DMDP) in 50 ml of 1.93×10^{-5} M PbI_2 solution (containing 9.65×10^{-7} mol Pb^{2+}). Thus, the amount of DMDP is roughly 2.5 times greater than that of Pb^{2+} in water. In addition, this concentration of PbI_2 solution also assures no solid PbI_2 in the solution because the maximum solubility of PbI_2 in water is 1.64×10^{-3} M, equivalent to about 340 ppm Pb^{2+} at room temperature. Figure 1d shows the temporal Pb^{2+} concentration profile of 50 ml of 1.93×10^{-5} M PbI_2 aqueous solution upon adding a 4-cm^2, 2.36-μm-thick DMDP film. Within about 30–60 min, the DMDP film was capable of depleting the Pb^{2+} concentration to below the detection limit (about 0.08 ppm) of our

[1]Department of Chemistry and Biochemistry, Northern Illinois University, DeKalb, IL, USA. [2]Chemistry and Nanoscience Center, National Renewable Energy Laboratory, Golden, CO, USA. [3]Materials Science Center, National Renewable Energy Laboratory, Golden, CO, USA. [4]Present address: Department of Physics and Astronomy, Valparaiso University, Valparaiso, IN, USA. [5]These authors contributed equally: Xun Li, Fei Zhang. ✉e-mail: Kai.Zhu@nrel.gov; txu@niu.edu

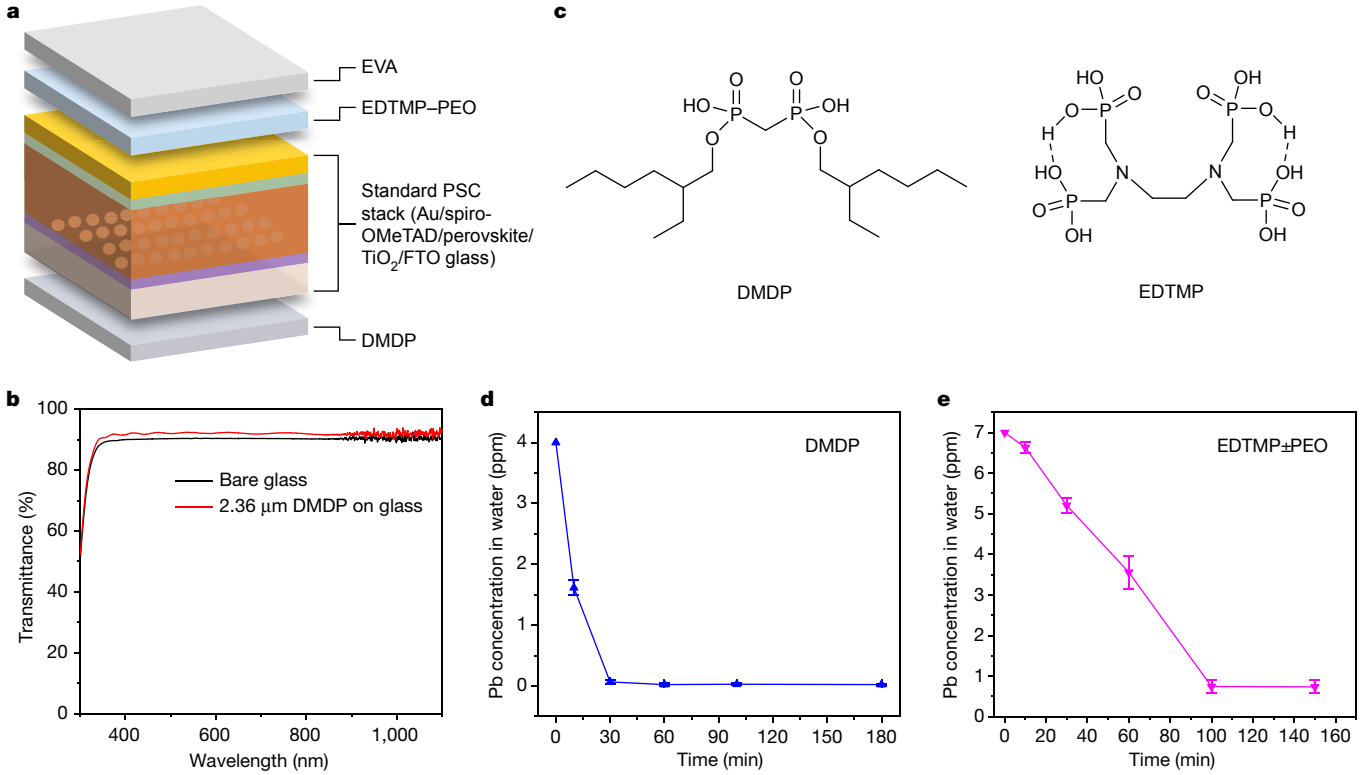

Fig. 1 | Device schematic and Pb-absorbing material properties. **a**, Illustration of adding Pb-absorbing materials—DMDP film and EDTMP–PEO film—on the front (glass) and back (metal electrode) sides, respectively, of a standard n–i–p PSC (FTO glass/TiO_2/perovskite/spiro-OMeTAD/Au). The EDTMP–PEO film is further covered by an EVA layer. **b**, Optical transmittance of glass substrate with and without the coating of 2.36-μm-thick DMDP layer. **c**, Molecular structures of DMDP and EDTMP used as the Pb-absorbing materials. **d**, **e**, Demonstration of Pb-absorbing capabilities of 4-cm^2 DMDP and EDTMP–PEO films soaked in 50 ml PbI_2 aqueous solutions. The error bars represent the standard deviations from five DMDP samples and three EDTMP–PEO samples. For DMDP, the film thickness is 2.36 μm and the initial PbI_2 solution concentration is 1.93×10^{-5} M (equivalent to a total of 9.65×10^{-7} mol Pb^{2+} or 4 ppm of Pb^{2+}). For EDTMP–PEO, EDTMP mixed with PEO in ACN was used to prepare the coating with 0.01 g cm^{-2} EDTMP in the final film, and the initial Pb concentration in PbI_2 solution is 7 ppm.

atomic absorption spectrometer. Varying the DMDP film thickness from 1.97 to 6.89 μm showed no notable effect on the Pb^{2+}-absorbing capability (Extended Data Fig. 4a). In contrast, the 0.7-μm-thick DMDP film (equivalent to about 75% of the amount of Pb^{2+} in solution) showed limited effect due to insufficient binding sites. For the rest of this study, we chose to use a 2.36-μm-thick DMDP film for further systematic measurements.

As directly applying DMDP in ethanol solution on the back (metal) side of the device causes damage to the perovskite stack (Extended Data Fig. 5), we used a pre-dry film on the back side comprising a mixture of strong commodity Pb-chelating agents (for example, *N*,*N*,*N*′,*N*′-ethyl enediaminetetrakis(methylenephosphonic acid), or EDTMP; Fig. 1c) blended in a host polymer matrix to ensure that the chelating agents alone or the formed Pb-chelating complex cannot be washed off by water. Although the EDTMP–polymer blend is opaque, transparency is not a concern for the Pb-sequestrating material on the back side in this study. The binding energy of EDTMP with Pb^{2+} is calculated to be 252.6 kJ mol^{-1} (Extended Data Fig. 2), which is 43 kJ mol^{-1} lower than that of DMDP. We found that using poly(ethylene oxide) (PEO; viscosity-average molecular weight, 2,000,000), along with acetonitrile (ACN) as the solvent, is an effective way to form an EDTMP–PEO blended film with good Pb-absorbing capability (Fig. 1e). More details on the polymer and solvent selection are given in Extended Data Fig. 4b.

We integrated these two Pb-absorbing films into PSCs (Fig. 1a) and investigated their effects on the capability of on-device Pb sequestration. A 2.36-μm-thick DMDP film and an EDTMP–PEO film (containing 2.3×10^{-5} mol cm^{-2} EDTMP) were installed on the front and back side, respectively, of the PSCs, with a total perovskite covered area of 2.5 cm × 2.5 cm; identical pristine devices were used for comparison. The perovskite composition is $(CsPbI_3)_{0.05}(FAPbI_3)_{0.85}(MAPbBr_3)_{0.15}$ (where, $CsPbI_3$ is caesium lead iodide, $FAPbI_3$ is formamidinium lead iodide and $MAPbBr_3$ is methylammonium lead bromide). Note that an ethylene vinyl acetate (EVA) film is applied to cover the back side for all PSCs unless otherwise stated. The use of EVA coating does not affect the device current density–voltage (*J*–*V*) characteristics (Extended Data Fig. 6). We forcefully shattered the glass side using a hammer and cut through the EVA film and underneath layers from the back side using a razor blade for all tested PSCs in the same manner and patterns (see photographs in Fig. 2a and detailed cell-damaging procedures with Pb sequestration results in Extended Data Fig. 7). Then, all devices were soaked in identical beakers containing 40 ml of pure water for the Pb-leaking and -sequestration study. Figure 2b shows the time-dependent Pb concentration when soaking the two-side damaged devices coated with Pb-absorbing films in 40 ml of pure water, compared with similarly damaged pristine devices. These studies were conducted at both room temperature and 50 °C (to enhance the Pb leakage rate) and repeated for six devices for each condition. With the on-device Pb-absorbing films, the Pb leakage from the devices soaked in water was about 0.2 ppm, at both temperatures, suggesting that the Pb-absorbing films can effectively capture most of the leaked Pb ions from the Pb-containing perovskite layer in PSCs. A computational model based on the diffusion equation also demonstrated a substantial contrast in Pb leakage with and without the DMDP Pb-absorbing film (Extended Data Fig. 8). The sequestration efficiency (SQE) was calculated only for devices with Pb-absorbing films installed on both sides of the device, and is defined by

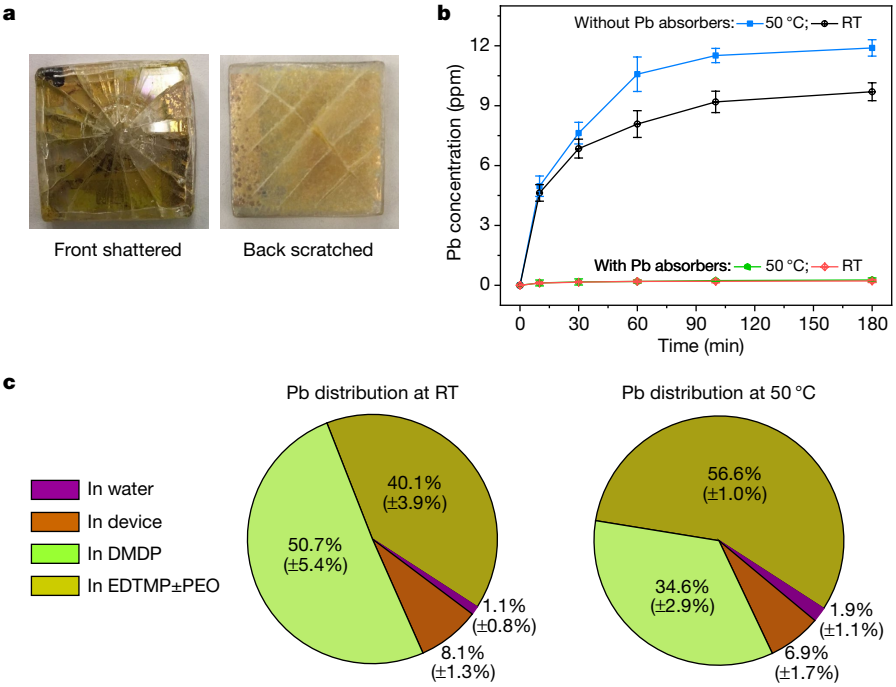

Fig. 2 | On-device Pb-sequestration capability. a, Photographs showing the two sides of damaged PSCs. **b**, Pb-leaking measurement and comparison of the Pb sequestration for the damaged PSCs with and without the Pb-absorbing layers. The results show the Pb-sequestration effect of DMDP and EDTMP–PEO coatings on PSCs. The damaged PSCs (2.5 cm × 2.5 cm) were soaked in 40 ml of pure water at room temperature (RT) and 50 °C. The error bars represent the standard deviations from six samples for each type of condition. All devices were covered with an EVA layer on the metal-electrode side. **c**, Distribution of Pb percentage found at various locations as indicated for two-side damaged PSCs containing Pb-absorbing layers on both sides of the device after a 3 h soaking in 40 ml of pure water. Note that the undissolved Pb left over in the device is denoted as 'in device'. The averages and standard deviations based on four devices for each type of sample are indicated.

$\mathrm{SQE}(\%) = \left(1 - \frac{\text{Pb leakage from devices with Pb absorbers on both sides}}{\text{Pb leakage from devices without any Pb absorbers}}\right)100\%$. Consequently, the SQE for a device with two sides coated in Pb-sequestrating films soaked in pure water is on average about 97.7% at room temperature and about 97.8% at 50 °C.

We further studied the Pb-sequestration behaviour in acidic water (pH = 4.2, simulating acidic rain conditions), water with an additional competing ion (0.1 ppm Ca^{2+}, which is chosen based on the typical reported concentration of Ca^{2+} in rainwater[30]) and flowing water (simulating heavy-rain conditions). The Pb SQE after a 3 h soaking test in acidic water averaged about 96.1% and 97.7% at room temperature and 50 °C (Extended Data Fig. 9a, b), respectively; these results are comparable to those obtained from leakage tests in pure water. In addition, no obvious negative effect of the competitive ion (Ca^{2+}) on Pb sequestration was observed (Extended Data Fig. 9c, d). To simulate the condition of flowing water (heavy rainfall, 50 mm h^{-1}; ref. [27]), two types of water—pure water and acidic water (pH = 4.2)—were used (Extended Data Fig. 9e, f). The Pb SQE was found to be in the range of 96.6–97.9% for pure water and in a similar range of 96.7–98.1% for acidic water. These results also suggest that water-induced swelling of the Pb-absorbing films does not restrict Pb^{2+} access to the available binding sites, precluding saturation of the Pb-sequestration effect by excessive hydration.

To track the outflow of Pb^{2+}, we also studied the amounts of Pb^{2+} in both of the Pb-sequestrating films as well as the amount left over in the two-side damaged devices after 3 h of soaking in 40 ml of pure water at both room temperature and 50 °C. The distribution of the Pb percentage found at various locations is shown in Fig. 2c. Interestingly, DMDP absorbs more Pb at room temperature, whereas EDTMP–PEO absorbs more Pb at 50 °C. At a higher temperature, the amount of deprotonated Pb-absorbing species increases relative to the neutral ones. Our density functional theory calculations (Extended Data Fig. 2) show that the Pb-binding energies are higher for the deprotonated species compared with the neutral ones, where Pb forms bonds with three oxygens. The free-energy change of chelating Pb^{2+} is more negative for the deprotonated EDTMP than DMDP, which makes the binding towards EDTMP more favourable.

To systematically evaluate the impact of our on-device Pb-sequestration schemes on the photovoltaic performance of PSCs, we compared the PSCs in a sequence of three different configurations: (1) pristine control PSC devices; (2) adding a transparent DMDP layer on the glass side of the PSC devices; and (3) adding an additional EDTMP–PEO layer on the metal-electrode side. All devices are covered by the EVA packaging film. Figure 3a, b shows the *J*–*V* curves and the corresponding incident photon-to-electron conversion efficiency (IPCE) of representative devices measured in the sequence of the above three configurations. All *J*–*V* curves with both forward and backward voltage scans in the three configurations essentially overlap with each other, suggesting no negative impact of adding Pb-absorbing layers on PSC performance. The details of the photovoltaic parameters from these *J*–*V* curves and the statistical comparison of the device parameters are shown in Extended Data Fig. 10. The stable power output efficiencies were also examined (Fig. 3c) and the results are consistent with the *J*–*V* measurements, which can be attributed to the minimum hysteresis observed for these devices (Fig. 3a). It is worth noting that the use of the DMDP layer exhibited negligible impact on the device performance and the integrated current density from IPCE spectra showed a range of 22.2–22.4 mA cm^{-2}, which further confirms that the coating of DMDP does not have substantial impact on the optical properties of the devices. Finally, we studied the long-term stability of these devices under continuous operation at simulated 1 sun illumination intensity in air at about 50 °C. No difference in device performance was observed after about 500 h of continuous operation (Fig. 3d). These results indicate that using the Pb-absorbing layers (especially the DMDP film, which is within the direct optical path

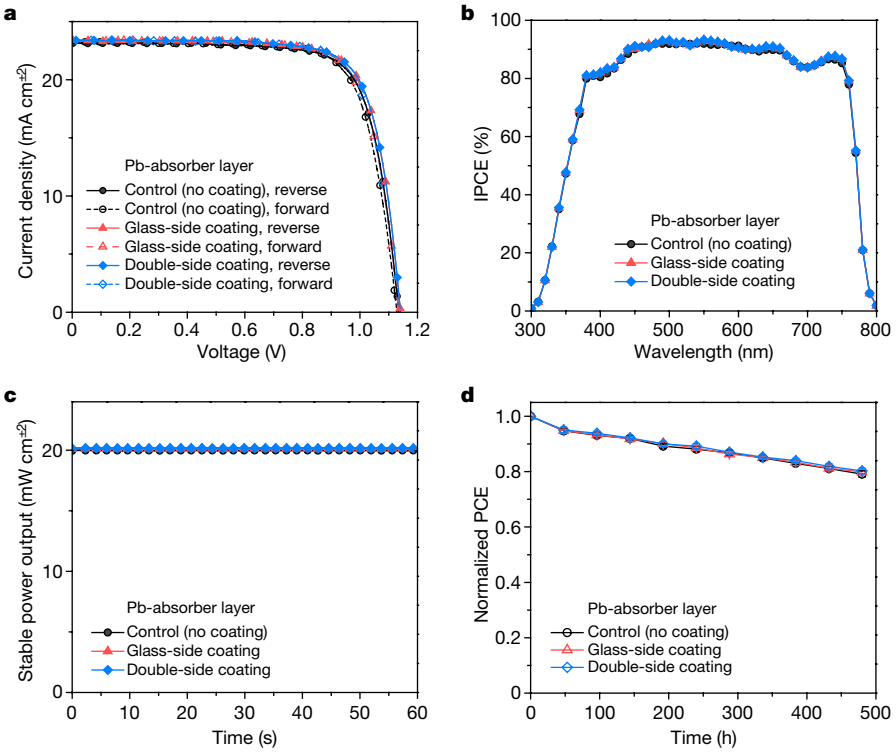

Fig. 3 | Device performance. a–d, Comparison of the *J*–*V* characteristics (**a**), IPCE (**b**), stable power output (**c**) and operation stability (**d**) for PSCs prepared with and without the Pb-absorbing layers. All devices are covered by an EVA layer. PCE, power conversion efficiency.

of the incident light) does not negatively impact device performance and long-term operation stability.

Online content

Any methods, additional references, Nature Research reporting summaries, source data, extended data, supplementary information, acknowledgements, peer review information; details of author contributions and competing interests; and statements of data and code availability are available at https://doi.org/10.1038/s41586-020-2001-x.

1. *Best Research-Cell Efficiency Chart* (National Renewable Energy Laboratory, 2019); https://www.nrel.gov/pv/cell-efficiency.html
2. Rong, Y. et al. Challenges for commercializing perovskite solar cells. *Science* **361**, eaat8235 (2018).
3. Park, N.-G., Grätzel, M., Miyasaka, T., Zhu, K. & Emery, K. Towards stable and commercially available perovskite solar cells. *Nat. Energy* **1**, 16152 (2016).
4. Jena, A. K., Kulkarni, A. & Miyasaka, T. Halide perovskite photovoltaics: background, status, and future prospects. *Chem. Rev.* **119**, 3036–3103 (2019).
5. Green, M. A., Ho-Baillie, A. & Snaith, H. J. The emergence of perovskite solar cells. *Nat. Photon.* **8**, 506–514 (2014).
6. Burschka, J. et al. Sequential deposition as a route to high-performance perovskite-sensitized solar cells. *Nature* **499**, 316–319 (2013).
7. Christians, J. A., Habisreutinger, S. N., Berry, J. J. & Luther, J. M. Stability in perovskite photovoltaics: a paradigm for newfangled technologies. *ACS Energy Lett.* **3**, 2136–2143 (2018).
8. Saparov, B. & Mitzi, D. B. Organic–inorganic perovskites: structural versatility for functional materials design. *Chem. Rev.* **116**, 4558–4596 (2016).
9. Correa-Baena, J.-P. et al. Promises and challenges of perovskite solar cells. *Science* **358**, 739–744 (2017).
10. Wang, R. et al. A review of perovskites solar cell stability. *Adv. Funct. Mater.* **29**, 1808843 (2019).
11. Bae, S.-Y. et al. Hazard potential of perovskite solar cell technology for potential implementation of "safe-by-design" approach. *Sci. Rep.* **9**, 4242 (2019).
12. Lyu, M., Yun, J.-H., Chen, P., Hao, M. & Wang, L. Addressing toxicity of lead: progress and applications of low-toxic metal halide perovskites and their derivatives. *Adv. Energy Mater.* **7**, 1602512 (2017).
13. Hailegnaw, B., Kirmayer, S., Edri, E., Hodes, G. & Cahen, D. Rain on methylammonium lead iodide based perovskites: possible environmental effects of perovskite solar cells. *J. Phys. Chem. Lett.* **6**, 1543–1547 (2015).
14. Fabini, D. Quantifying the potential for lead pollution from halide perovskite photovoltaics. *J. Phys. Chem. Lett.* **6**, 3546–3548 (2015).
15. Babayigit, A., Ethirajan, A., Muller, M. & Conings, B. Toxicity of organometal halide perovskite solar cells. *Nat. Mater.* **15**, 247–251 (2016).
16. Babayigit, A., Boyen, H.-G. & Conings, B. Environment versus sustainable energy: the case of lead halide perovskite-based solar cells. *MRS Energy Sustain.* **5**, E1 (2018).
17. Wei, M. et al. Ultrafast narrowband exciton routing within layered perovskite nanoplatelets enables low-loss luminescent solar concentrators. *Nat. Energy* **4**, 197–205 (2019).
18. Cannavale, A. et al. Perovskite photovoltachromic cells for building integration. *Energy Environ. Sci.* **8**, 1578–1584 (2015).
19. Wheeler, L. M. et al. Switchable photovoltaic windows enabled by reversible photothermal complex dissociation from methylammonium lead iodide. *Nat. Commun.* **8**, 1722 (2017).
20. Lin, J. et al. Thermochromic halide perovskite solar cells. *Nat. Mater.* **17**, 261–267 (2018).
21. Polman, A., Knight, M., Garnett, E. C., Ehrler, B. & Sinke, W. C. Photovoltaic materials: present efficiencies and future challenges. *Science* **352**, aad4424 (2016).
22. Ramírez Quiroz, C. O. et al. Pushing efficiency limits for semitransparent perovskite solar cells. *J. Mater. Chem. A* **3**, 24071–24081 (2015).
23. Meinardi, F., Bruni, F. & Brovelli, S. Luminescent solar concentrators for building-integrated photovoltaics. *Nat. Rev. Mater.* **2**, 17072 (2017).
24. Stoumpos, C. C., Malliakas, C. D. & Kanatzidis, M. G. Semiconducting tin and lead iodide perovskites with organic cations: phase transitions, high mobilities, and near-infrared photoluminescent properties. *Inorg. Chem.* **52**, 9019–9038 (2013).
25. van der Voet, E. et al. *Environmental Challenges of Anthropogenic Metals Flows and Cycles* (United Nations Environment Programme, 2013).
26. *Lead Laws and Regulations* https://www.epa.gov/lead/lead-laws-and-regulations (Environmental Protection Agency, 2019).
27. Jiang, Y. et al. Reduction of lead leakage from damaged lead halide perovskite solar modules using self-healing polymer-based encapsulation. *Nat. Energy* **4**, 585–593 (2019).
28. Conings, B., Babayigit, A. & Boyen, H.-G. Fire safety of lead halide perovskite photovoltaics. *ACS Energy Lett.* **4**, 873–878 (2019).
29. Current results weather and science facts: average annual precipitation by state. *Current Results* https://www.currentresults.com/Weather/US/average-annual-state-precipitation.php (2019).
30. Bormann, B. T., Tarrant, R. F., McClellan, M. H. & Savage, T. Chemistry of rainwater and cloud water at remote sites in Alaska and Oregon. *J. Environ. Qual.* **18**, 149–152 (1989).

Methods

Materials

All solvents and other chemicals were used as received without further refinement unless otherwise noted. DMDP was purchased from Eichrom Technologies. Formamidinium iodide (FAI) and methylammonium bromide (MABr) were purchased from Greatcell Solar. Lead(II) iodide (PbI_2), lead(II) bromide ($PbBr_2$) and EDTMP were purchased from TCI. 2,2′,7,7′-Tetrakis[*N*,*N*-di(4-methoxyphenyl)amino]-9,9′-spirobifluorene (spiro-OMeTAD) was purchased from Merck Corporation. The titanium diisopropoxide bis(acetylacetonate), *tert*-butylpyridine, bis(trifluoromethanesulfonyl)imide lithium salt, caesium iodide (CsI), PEO (average viscosity average molecular weight, about 2,000,000) and poly(vinyl alcohol) (average molecular weight, 86,000) were purchased from Sigma-Aldrich. The solar-grade EVA film was purchased from Amazon. The patterned fluorine-doped tin-oxide (FTO)-coated glass substrates (<15 Ω per square) were obtained from Advanced Election Technology.

Device fabrication

Devices were prepared on conductive FTO glass substrates. The substrates were cleaned by the cleaner, isopropanol, acetone and ethanol, during which the substrates were also rinsed by deionized water in between each step. A thickness of about 40 nm of compact titanium dioxide was deposited by spray pyrolysis of 7 ml isopropanol solution, which contains 0.6 ml titanium diisopropoxide bis(acetylacetonate) solution (75% in isopropanol, Sigma-Aldrich) and 0.4 ml acetylacetone at 450 °C in air. Then, a layer of mesoporous titanium dioxide with 30-nm-sized nanoparticles (30NRD, Dyesol) moderated in ethanol (1:6 w/w) was spin-coated at 4,500 r.p.m. for 15 s on this layer, followed by heating at 500 °C for 0.5 h in air. The precursors of $[(CsPbI_3)_{0.05}(FAPbI_3)_{0.85}(MAPbBr_3)_{0.15}]$ were dissolved in a mixed solvent of dimethylformamide and dimethylsulfoxide (4:1 v/v) and prepared in a glovebox to form a 1.4 M Pb^{2+} (PbI_2 and $PbBr_2$) solution. For the perovskite film, a spin-coating procedure was executed at 2,000 r.p.m. for the first 10 s, followed by 6,000 r.p.m. for the second 30 s. At 15 s before the end of the spin-coating procedure, 140 µl of chlorobenzene was dropped on the substrates. The substrates were then annealed on a hotplate at 100 °C for 1 h on a covered Petri dish. Subsequently, the spiro-OMeTAD solution, as a hole-transporting material, was prepared by dissolving the spiro-OMeTAD in 1 ml chlorobenzene at a concentration of 60 mM with the addition of 30 mM bis(trifluoromethanesulfonyl)imide lithium salt from a stock solution in ACN and 200 mM of *tert*-butylpyridine[31]. The spiro-OMeTAD solution was deposited on top of the perovskite surface by spin-coating at 4,000 r.p.m. for 15 s. Finally, the devices were completed by thermal evaporation of 100 nm gold as the metal contact.

PSC packaging

All solar cells were treated in three conditions: (1) pristine devices only packaged by an EVA film on the metal side; (2) devices with a DMDP film on the glass side and an EVA film on the metal side; and (3) devices with a DMDP film on the glass side and an EDTMP–PEO film on the metal side followed by an EVA film. Devices of the first case were used as the control samples without any further processing. For the second case, the DMDP film was formed by spin-coating 0.38 M DMDP in ethanol solution on the glass side at 1,000 r.p.m. for 10 s. For the third case, the metal side was packed by EVA film with an EDTMP–PEO film in between. The EVA film was softened to seal the edge of devices by heat treatment, and the extra films on the edge were cut off to be flush with the glass surface. The EDTMP–PEO films were made by blending PEO with EDTMP. Briefly, PEO was dissolved in ACN at a concentration of 10 wt%; the gel-like PEO solution was physically mixed with EDTMP fine powder under vigorous mechanical stirring. The resulting opaque mixture was doctor-bladed on a plastic plate, followed by desiccation, to form a PEO film containing 0.01 g cm^{-2} of EDTMP, denoted as EDTPM–PEO film, which was peeled off and cut into the same area as the perovskite layer and sandwiched between the metal electrodes and EVA film. The thickness (about 0.45 mm) of the dried EDTMP–PEO film was determined by a micrometer. Thereafter, the devices were spin-coated with DMDP solution on the glass side. A schematic of the assembly process is given in Extended Data Fig. 5.

PSC characterization

Simulated AM 1.5G illumination with a power density of 100 mW cm^{-2} (Oriel Sol3A Class AAA Solar Simulator) was used to measure the solar cell performance. The *J*–*V* characteristic curves were tested using a Keithley 2400 source meter. The *J*–*V* characteristic curves of all solar cells were measured by employing a metal mask with an active area of 0.12 cm^2. Scan curves, both backward and forward, were tested with a bias step fixed at 10 mV and delay time fixed at 0.05 s. A potentiostat (Princeton Applied Research, Versa STAT MC) was employed to measure the continuous current and power output. The IPCE spectra of the solar cells were measured using a solar cell quantum-efficiency measurement system (QEX10, PV Measurements). The film thickness of the perovskite layer was determined from the cross-section scanning electron microscopy image (FEI Nova 630, field-emission gun), obtained with an electron-beam voltage of 3 kV and current of 3 nA in the immersion-lens mode.

Pb-absorption characterization

Optical transmission spectroscopy was carried out with an ultraviolet–visible spectrophotometer (UV-2600, Shimadzu Scientific Instruments) at a spectral range of 300–1,100 nm. The prepared DMDP solutions with concentrations of 0.19, 0.38, 0.57 and 0.76 M to attain different thicknesses were spin-coated on the glass substrates (VWR International) at 1,000 r.p.m. for 10 s for subsequent transmittance measurements. Note that it is difficult to form a free-standing DMDP film, for example, by peeling the DMDP film (after solvent evaporation) off a substrate (for example, glass or plastic plate) without breaking it because the film is very sticky to the substrate. The thickness of the DMDP film is determined by a combination of micrometer and mass difference. In brief, we first determine the density of the DMDP film (about 1.05 g ml^{-1}) by preparing a relatively thick DMDP film on a cover glass with a known thickness and mass. We then determine the total mass and thickness of the cover glass covered with the DMDP film. Knowing the area, thickness and mass, we can determine the density of the DMDP film. Thus, the thickness of DMDP films prepared with different conditions can be determined by the mass difference method with the knowledge of film density and area.

Flame atomic absorption spectrophotometry (FAAS) was conducted with an AA-6200 (Shimadzu Scientific Instruments), equipped with a Pb hollow-cathode lamp as a radiation source, where the resonance line wavelength is 217 nm. An air/acetylene flame with a fuel rate of 2 l min^{-1}, lamp current of 12 mA and a slit width of 0.7 nm under the BGC-D2 mode were applied. A calibration curve based on PbI_2 solutions was referenced by all sample tests to determine the aqueous Pb content in pure water as a standard.

For preliminary evaluation of the absorption capacity of DMDP, 2 cm × 2 cm areas of glass substrates were first spin-coated with DMDP solutions. For each concentration, gradient spin rates, ranging from 500 to 4,000 r.p.m., were employed to form the transparent layers with different thicknesses. Then, each DMDP-coated glass substrate was dipped into 50 ml of 4 ppm aqueous PbI_2 solutions for time-dependent Pb-absorption measurements. Similarly, for preliminary evaluation of Pb-absorbing films (for example, EDTMP–PEO) used on the metal-electrode side, each film with an area of 2 cm × 2 cm was soaked in 50 ml of 7 ppm aqueous PbI_2 solutions for time-dependent Pb-absorption measurements.

We followed four steps to determine the distribution of the Pb content in various locations during the Pb-leakage test with damaged PSCs

installed with DMDP and EDTMP–PEO films. (1) Two-side damaged devices were soaked in 40 ml of water in a plastic beaker. After 3 h, the water in the beaker was tested to determine the amount of leaked Pb^{2+} in water by FAAS. (2) The device was taken out of the beaker and disassembled by carefully peeling off the EVA film from the device edges, followed by isolating the EDTMP–PEO film from the EVA film and device. The peeled-off EDTMP–PEO film was placed in a quartz beaker and burned by a torch flame into black ashes. Then 20 ml of 1 M HNO_3 solution was added to the beaker and heated to 70 °C for 3 h to extract the Pb content from the ashes. The amount of Pb was then determined by FAAS. (3) The shattered glass pieces were carefully picked up using a plastic tweezer. The glass pieces were further soaked by submerging them in water in a new clean plastic beaker with the perovskite side facing down to avoid re-absorption of residual Pb^{2+} by DMDP if it touches water. The water collected in this new beaker was diluted with water up to 10 ml, and FAAS was used to measure the Pb amount, giving rise to the residual undissolved Pb amount in the device. (4) The Pb amount in the DMDP film was obtained by subtracting the above three Pb amounts from the total amount of the Pb in a device as statistically confirmed in Extended Data Fig. 3.

Computational method

Electronic structure calculations based on the density functional theory were performed with the B3LYP functional form[32,33], together with the LANL2DZ basis set for Pb and the 6-31+G(d,p) basis sets for all the other elements using the program package Gaussian 09[34]. Contributions from van der Waals dispersion forces were included in the form of the Grimme-D2 terms in the calculations[35]. The polarizable continuum model[36] was used to mimic the solvent effect, which calculates the energy in solution by making the solvent reaction field self-consistent with the solute electrostatic potential generated from the calculated electron density. For water, a dielectric constant $\varepsilon = 78.35$ was used. The geometry optimization was done without applying any constraints. The convergence criteria in maximum force, root mean square force, maximum displacement and root mean square displacement were set as 0.023 eV Å^{-1}, 0.015 eV Å^{-1}, 9.5×10^{-4} Å and 6.4×10^{-4} Å, respectively. The electronic binding energy, E_b, of the Pb^{2+} ion with a DMDP or EDTMP molecule was calculated as:

$$E_b = (E_{molecule} + E_{Pb}) - E_{Pb-molecule} \quad (1)$$

where $E_{Pb-molecule}$, E_{Pb} and $E_{molecule}$ are the total energies of the Pb^{2+}–molecule conjugate, Pb^{2+} ion, and the DMDP or EDTMP molecule, respectively. The more positive the E_b value, the higher the stability of the conjugated complex. To take into account the temperature effect, we also calculated the Gibbs free-energy change of adsorption, which takes the convention of the total free energy of the conjugated complex minus the sum of free energies of the reactants. The more negative the free-energy change, the higher the equilibrium constant for adsorption. These values are reported in Extended Data Fig. 2.

Simulation of the variation in the concentration of Pb ions was conducted by considering the diffusion process of Pb in the bulk solution:

$$\frac{\partial}{\partial t} C(\mathbf{r}, t) = D\nabla^2 C(\mathbf{r}, t) \quad (2)$$

where D is the diffusion coefficient of Pb and $C(\mathbf{r}, t)$ represents the concentration of Pb in the bulk, where $\mathbf{r}$ and t are the position and time, respectively. This was done by solving the partial differential equation using the finite-element method as implemented in the program MATLAB. The value of D was set to 9.4×10^{-10} m^2 s^{-1} (ref. [37]), which is equivalent to 0.0564 mm^2 min^{-1}. This value was boosted ten times to achieve concentrations comparable to experiments in the case for the pristine control device. This is probably because some realistic factors such as convection are left out of our model. We compared two cases: the pristine control device (only sealed by EVA film on the metal-electrode side) and the device with DMDP on the glass side packaged by EVA on the metal-electrode side. The two devices were modelled by the same geometry in a two-dimensional model as shown in Extended Data Fig. 8a, b. The thickness of the glass was set to 1 mm. The bulk solution region was taken to be 3 mm wide and 1 mm thick. Upon shattering the glass side, small cracks were formed. We modelled such a crack using a typical width of 100 µm. The concentration of Pb^{2+} at the exposed perovskite site was set to the experimental value of 12.9 ppm measured for Pb concentration leaked from two-side damaged devices without any Pb-absorbing materials after being soaked in 40 ml of water for 3 h (Extended Data Fig. 3). The initial condition was set to zero everywhere else. The boundary conditions were set to the Neumann condition $\nabla C(\mathbf{r}, t) = 0$ everywhere except for the exposed perovskite boundary for the pristine device; for the DMDP-coated device, the Pb concentration at the boundary interfaced with DMDP was set to the Dirichlet condition $C(\mathbf{r}, t) = 0$, considering the high affinity of DMDP towards Pb. The simulated results are shown in Extended Data Fig. 8c, d for the cases without and with DMDP, respectively. In the absence of DMDP, the concentration of Pb is about 9.3 ppm in the bulk after 180 min, whereas it reduces to 0.5 ppm with the DMDP as an active Pb absorber.

Estimation of Pb content in a device

Here we show the estimation of the Pb content in PSCs with three different perovskite compositions. To calculate the Pb content in $MAPbI_3$, we need to use the molecular weight (620 g mol^{-1}), mass percentage of Pb (207/620 = 33.39%) and density (4.09 g cm^{-3})[24]. Thus, for a typical 550-nm-thick film, the mass of Pb per unit area is about 0.75 g m^{-2}. Similarly, for $FAPbI_3$ with 32.7% Pb mass percentage and 4.10 g cm^{-1} density (refs. [3,24]), the mass of Pb per unit area is about 0.74 g m^{-2}. For the mixed perovskite composition such as $(CsPbI_3)_{0.05}(FAPbI_3)_{0.85}(MAPbBr_3)_{0.15}$, the mass percentage of Pb is 33.7% and the density is about 4.12 g cm^{-3} estimated from the weighted average of a mixture of $MAPbBr_3$ (3.83 g cm^{-3})[38], $FAPbI_3$ (4.10 g cm^{-3})[24] and $CsPbI_3$ (5.39 g cm^{-3})[24]. Thus, the mass of Pb per unit area is about 0.76 g m^{-2}.

Data availability

The data that support the findings of this study are available from the corresponding authors upon reasonable request.

31. Zhang, F. et al. Self-seeding growth for perovskite solar cells with enhanced stability. *Joule* **3**, 1452–1463 (2019).
32. Lee, C., Yang, W. & Parr, R. G. Development of the Colle-Salvetti correlation-energy formula into a functional of the electron density. *Phys. Rev. B* **37**, 785–789 (1988).
33. Becke, A. D. Density-functional thermochemistry. III. The role of exact exchange. *J. Chem. Phys.* **98**, 5648–5652 (1993).
34. Frisch, M. J. et al. *Gaussian09* revision D.01 (Gaussian, 2009).
35. Grimme, S. Semiempirical GGA-type density functional constructed with a long-range dispersion correction. *J. Comput. Chem.* **27**, 1787–1799 (2006).
36. Tomasi, J., Mennucci, B. & Cammi, R. Quantum mechanical continuum solvation models. *Chem. Rev.* **105**, 2999–3094 (2005).
37. Sato, H., Yui, M. & Yoshikawa, H. Ionic diffusion coefficients of Cs^+, Pb^{2+}, Sm^{3+}, Ni^{2+}, SeO_4^{2-} and TcO_4^- in free water determined from conductivity measurements. *J. Nucl. Sci. Technol.* **33**, 950–955 (1996).
38. Leyden, M. R. et al. Methylammonium lead bromide perovskite light-emitting diodes by chemical vapor deposition. *J. Phys. Chem. Lett.* **8**, 3193–3198 (2017).

Acknowledgements T.X. acknowledges the support from the National Science Foundation (DMR 1806152). The work at the National Renewable Energy Laboratory was supported by the US Department of Energy under contract number DE-AC36-08GO28308 with Alliance for Sustainable Energy, Limited Liability Company (LLC), the Manager and Operator of the National Renewable Energy Laboratory. K.Z., F.Z. and J.J.B. acknowledge the support on perovskite synthesis and device fabrication and characterization from the De-risking Halide Perovskite Solar Cells programme of the National Center for Photovoltaics, funded by the US Department of Energy, Office of Energy Efficiency and Renewable Energy, Solar Energy Technologies Office. The views expressed in the article do not necessarily represent the views of the DOE or the US Government. The US Government retains and the publisher, by accepting the article for publication, acknowledges that the US Government retains a nonexclusive, paid-up, irrevocable, worldwide license to publish or reproduce the published form of this work, or allow others to do so, for US Government purposes.

Author contributions T.X. and K.Z. designed and supervised the research. X.L. prepared the Pb-absorbing materials and conducted the Pb-leaking and -capture characterization in films and devices. F.Z. fabricated and characterized the perovskite thin films and devices. H.H. conducted the theoretical calculation and simulation. J.J.B. conducted Pb impact analysis and a life-cycle assessment literature review. All authors discussed the results and contributed to manuscript preparation.

Competing interests An application has been made for a provisional patent (US patent application number 62/853,951) related to the subject matter of this manuscript.

Additional information

Correspondence and requests for materials should be addressed to K.Z. or T.X.

Peer review information *Nature* thanks Bert Conings, Peng Gao and Antonio Urbina for their contribution to the peer review of this work.

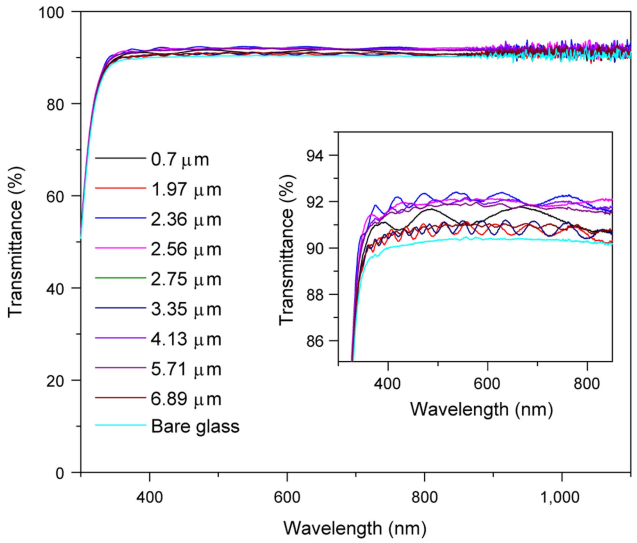

Extended Data Fig. 1 | Optical transmittance of DMDP films coated on glass. The DMDP film thickness was varied from 0.7 to 6.89 μm. The inset shows the magnified view of the transmittance spectra.

a

Neutral	E_b	ΔG (25°C)	ΔG (50°C)	Deprotonated	E_b	ΔG (25°C)	ΔG (50°C)
DMDP	-295.6	-245.2	-241.1	$DMDP^-$	-344.8	-289.3	-285.3
EDTMP	-252.6	-225.5	-223.7	$EDTMP^-$	-343.4	-303.0	-300.3

b

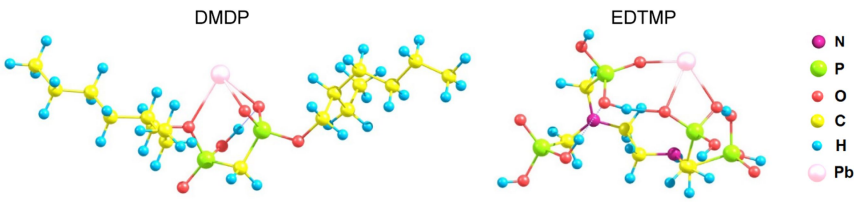

Extended Data Fig. 2 | Pb^{2+} binding energy. a, Calculation of both electronic binding energies (E_b) and Gibbs free-energy (ΔG) changes of adsorption of Pb^{2+} by neutral and deprotonated DMDP and EDTMP at room temperature (25 °C) and 50 °C. All energies are in units of kJ mol^{-1}. **b**, Schematic of binding configurations of Pb^{2+} ions with deprotonated DMDP and EDTMP. Configurations were obtained based on density functional theory calculations.

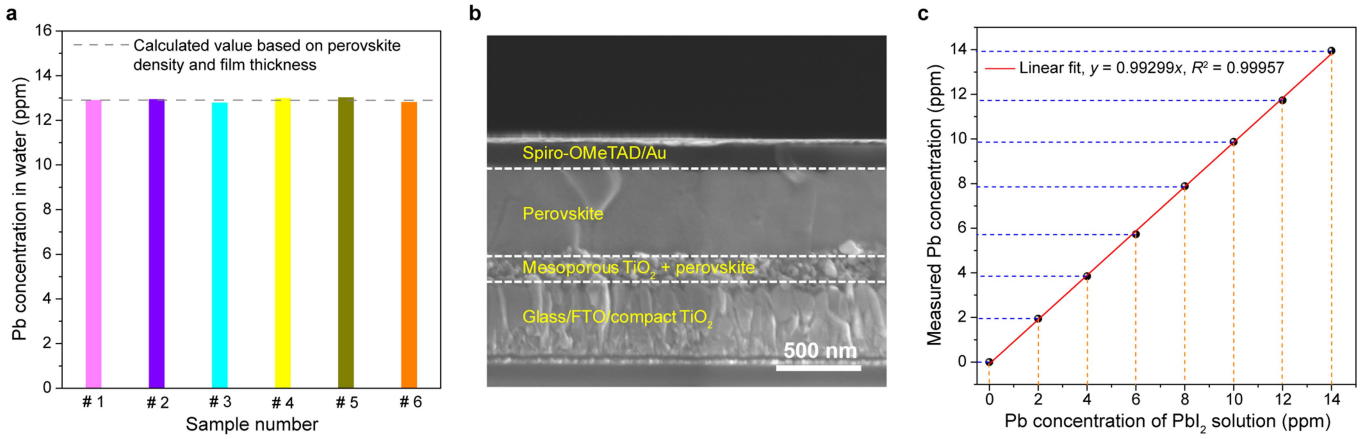

Extended Data Fig. 3 | Pb amount measurement verification. a, Pb concentration leaked from two-side damaged devices without any Pb-sequestrating materials and EVA packaging layer after being soaked in 40 ml of water for 3 h. Six devices were tested. The concentrations of dissolved Pb from these pristine devices were also calculated based on the density and thickness of the perovskite layers. **b**, Typical cross-sectional scanning electron microscopy image of the devices used in **a**. **c**, A typical verification curve of nominal Pb concentrations of various PbI_2 solutions and the measured concentrations by the flame atomic absorption spectrometer. The result shows excellent accuracy and precision of the measurement system.

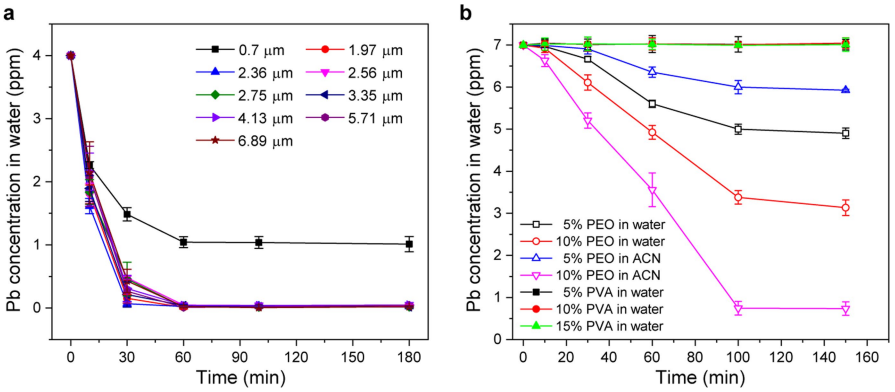

Extended Data Fig. 4 | Pb-sequestering performance of DMDP and EDTMP-blended films. a, Pb-sequestering performance as a function of soaking time for DMDP films coated on glass substrates. The DMDP film thicknesses are indicated. All DMDP films are soaked in 50 ml of 1.93×10^{-5} M PbI_2 aqueous solution (equivalent to 4 ppm of Pb^{2+}) to test their Pb-absorbing capability. Five samples were measured for 2.36-μm-thick DMDP and three samples were measured for other DMDP film thickness, with the averages and standard deviations (error bars) indicated. **b**, Evaluation of Pb-sequestering capabilities of different EDTMP-blended films prepared by various methods. Three samples of each configuration type were measured with the averages and standard deviations (error bars) indicated. The films were soaked in 50 ml of aqueous PbI_2 solution with a Pb concentration of 7 ppm. '5% PEO in water' stands for the film prepared by dissolving 5 wt% PEO (viscosity-average molecular weight, about 2,000,000) in pure water as solvent, followed by adding a proper amount of EDTMP under stirring. Then the mixture was smeared into a thin film using a doctor-blade coating method with such an area that the concentration of EDTMP is 0.01 g cm^{-2}. ACN was used as the test solvent. PVA, polyvinyl alcohol (molecular weight 86,000).

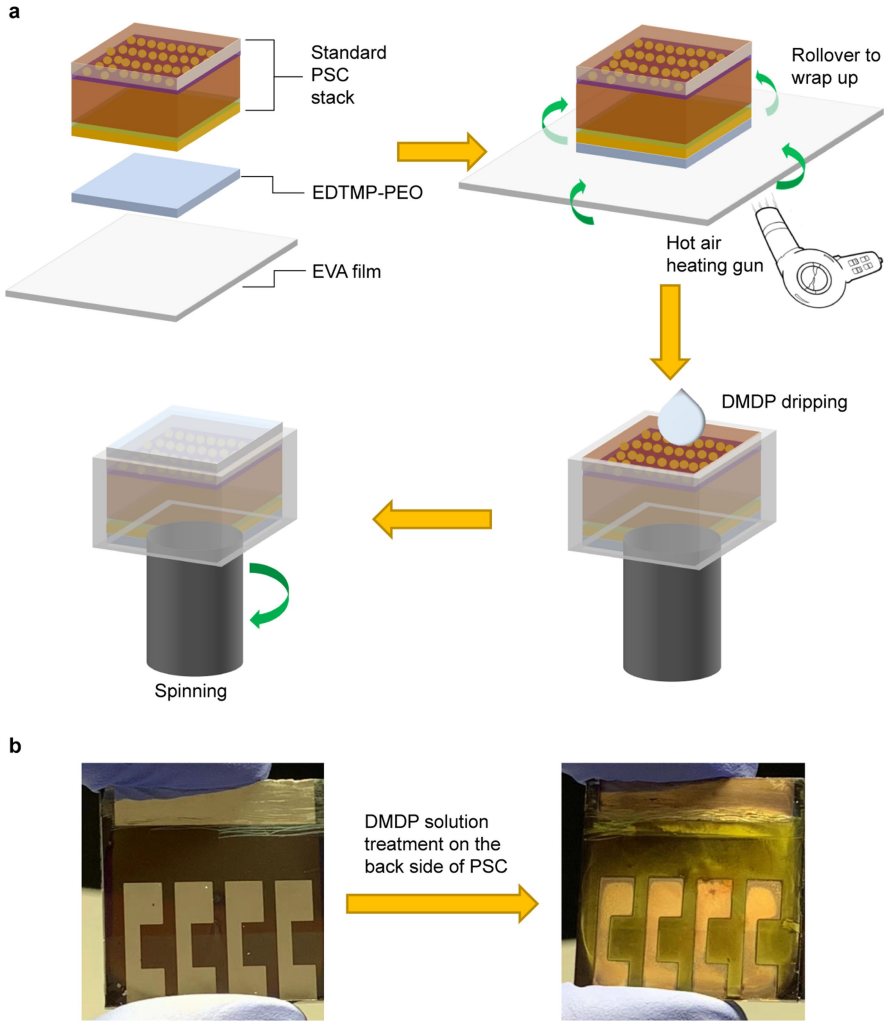

Extended Data Fig. 5 | Pb-sequestration films assembly processes. **a**, Schematic of integrating DMDP and EDTMP–PEO films into a PSC. **b**, Photos of a pristine device and a device treated with the DMDP solution showing that directly applying the DMDP in ethanol solution damaged the perovskite stack with evident yellowing associated with perovskite decomposition due to polar ethanol.

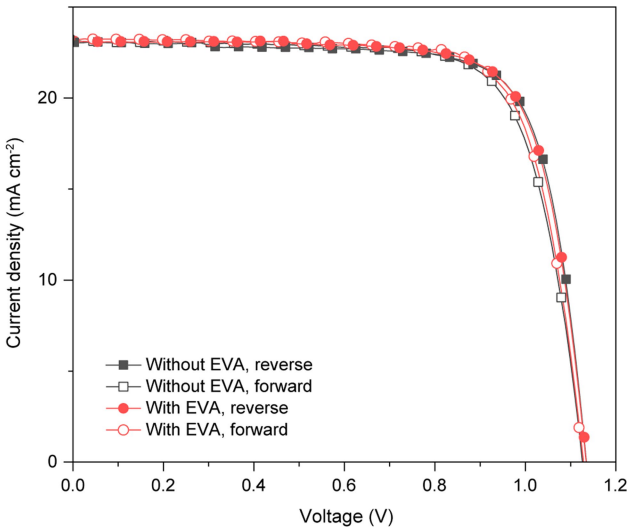

Extended Data Fig. 6 | EVA coating effect on device performance. *J*–*V* curves of PSCs with and without the EVA coating on the metal-electrode side of the device. Both forward- and reverse-voltage scans are shown. No clear impact on cell efficiency is observed for the EVA coating.

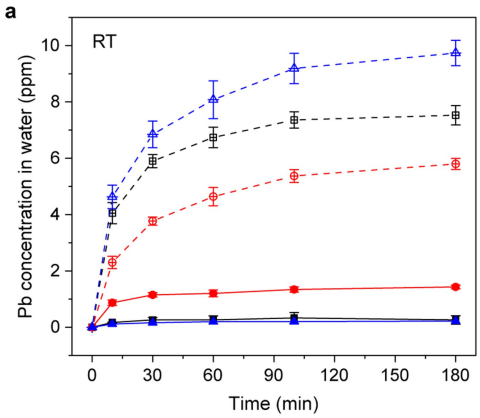

Sample Type	Front coating	Back coating	Front damage	Back damage
--△--	N	N	Y	Y
--□--	N	N	Y	N
--○--	N	N	N	Y
—●—	N	Y	N	Y
—■—	Y	N	Y	N
—▲—	Y	Y	Y	Y

Front: glass side; Back: metal side; Y: Yes; N: No

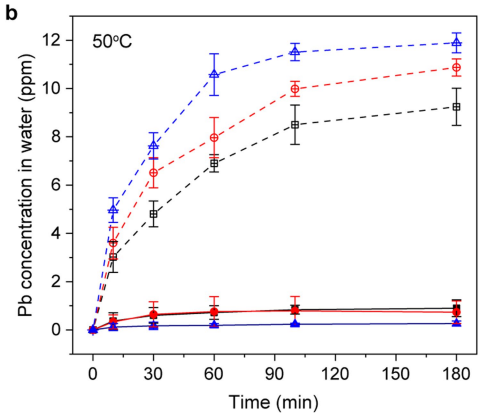

Sample Type	Front coating	Back coating	Front damage	Back damage
--△--	N	N	Y	Y
--□--	N	N	Y	N
--○--	N	N	N	Y
—●—	N	Y	N	Y
—■—	Y	N	Y	N
—▲—	Y	Y	Y	Y

Front: glass side; Back: metal side; Y: Yes; N: No

Extended Data Fig. 7 | Impact of device damage conditions on Pb sequestration in pure water. a,**b**, Six types of devices with different Pb-absorber layer coating and device damage conditions were tested. All devices were sealed by EVA film on the back metal-electrode side. The details of Pb-absorber coating and device-damage conditions are given in the table on the right. Six devices for each type of sample were tested. The Pb-leakage tests were conducted at room temperature (**a**) and 50 °C (**b**) by soaking each damaged device in 40 ml of water. The error bars represent the standard deviations from six samples of each type of device. It is worth noting that the case with both sides coated and damaged outperforms the case with only one side (particularly the back side) coated and damaged. This effect can be attributed to the chemical Pb-sequestrating nature of the DMDP and EDTMP–PEO films, which yields a summed sequestration effect, namely any aqueous Pb chemically captured by the Pb-sequestrating layer on one side will no longer flow back to the other side, hence, reducing the leaked Pb via either side compared with the case where a coating layer is present on only one side.

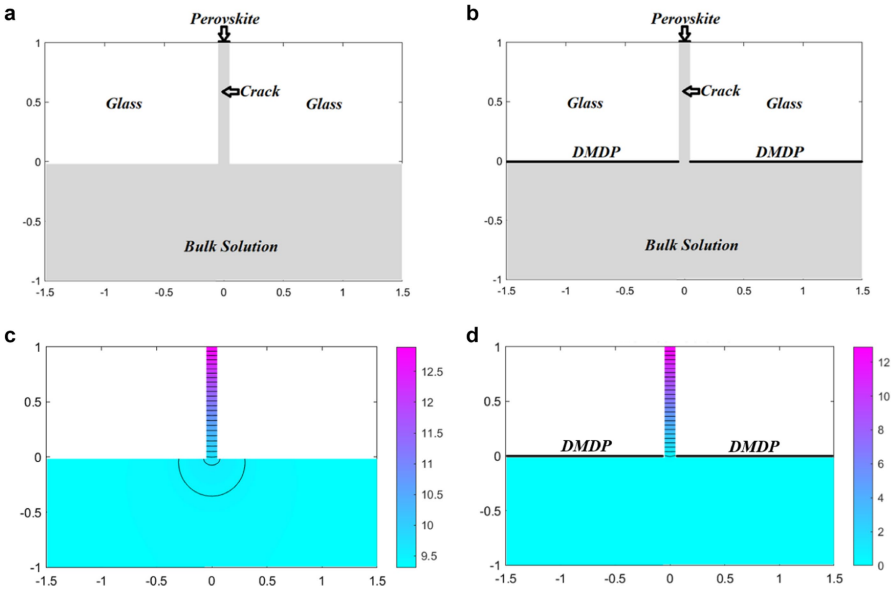

Extended Data Fig. 8 | Simulation of pristine and DMDP-coated devices on Pb sequestration at room temperature. a,**b**, The two-dimensional geometry models for a pristine control device (only covered by EVA film on the metal side; **a**) and a device including one coated with DMDP film on the glass-side alone (and the metal side is covered with EVA; **b**). **c**,**d**, The simulated spatial Pb concentrations for a pristine device (**c**) and a DMDP-coated device after 180 min of damage by shattering the glass side and forming cracks in the glass/DMDP (**d**). The labelled dimensions are in mm, and the colour-scale numbers are in ppm. Note that the colour scale ranges are different in **c** and **d**.

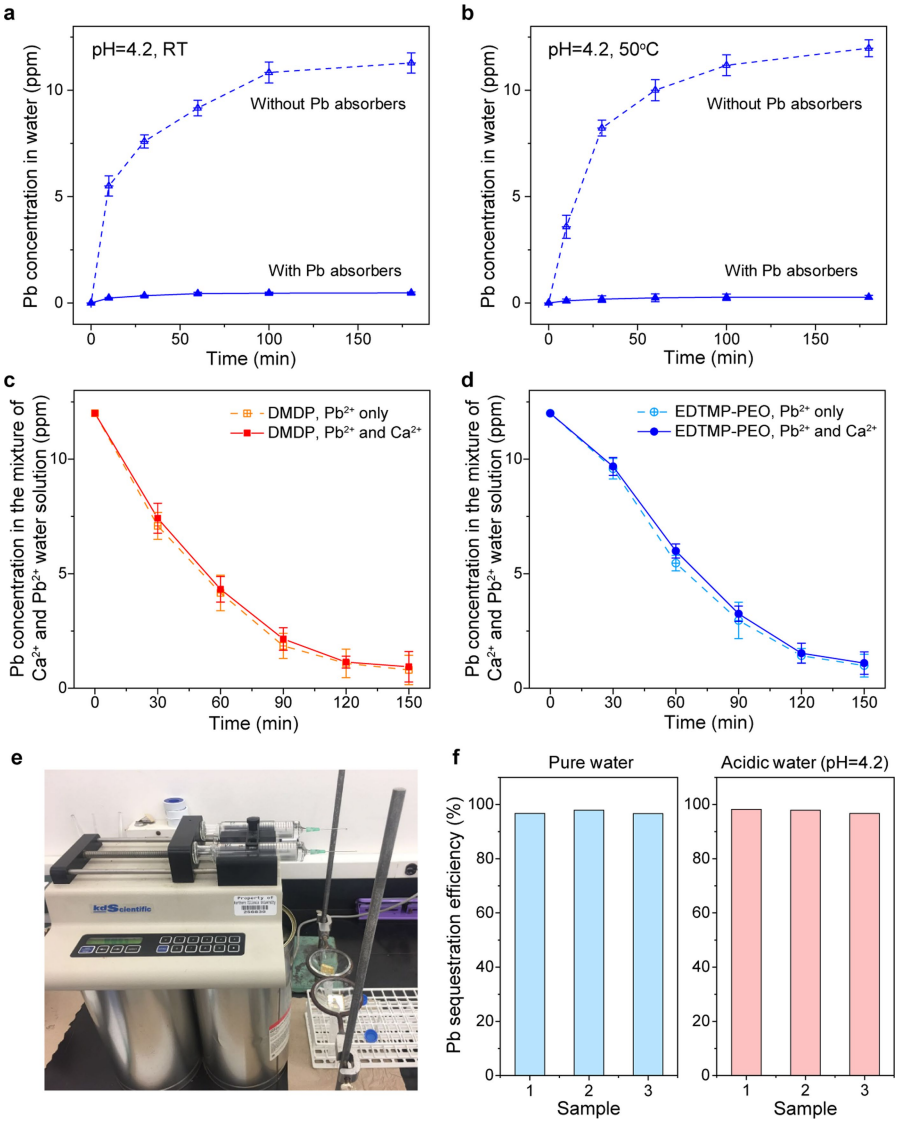

Extended Data Fig. 9 | Impact of acidic water, competitive ion (Ca^{2+}) and flowing water on Pb sequestration. a,**b**, Pb leakage of damaged PSCs in acidic water (pH = 4.2; 40 ml) at room temperature (**a**) and 50 °C (**b**). The samples with Pb absorbers have both sides of the device stack coated with the Pb-sequestrating films. All samples are covered by EVA film on the metal-electrode side. **c**,**d**, Effect of competitive ion Ca^{2+} (from $CaCl_2$) on Pb sequestration by DMDP (**c**) and EDTMP–PEO (**d**) samples using 40 ml water containing 12 ppm Pb^{2+} and 0.1 ppm Ca^{2+} at room temperature. For the control tests, the water solution contains only Pb^{2+} ions. The error bars in **a**–**d** represent the standard deviations from three devices of each type of test condition. **e**, Photograph of homemade apparatus to study Pb leakage from damaged devices under flowing water to simulate rainfall conditions. The flowing water is continuously dripped on the damaged devices at a rate of 5 ml h^{-1} for 1.5 h facilitated by a syringe pump. The damaged devices are placed in the funnel with a tilt angle of 30° versus horizon. The rinsed water that contains Pb is collected in plastic tubes. **f**, Comparison of Pb-sequestration efficiency of devices under flowing water at room temperature. All devices are installed with Pb absorbers on both sides. Three devices for each type of test condition were measured.

a

Sample	V_{oc} (V)	J_{sc} (mA cm^{-2})	FF	PCE (%)
Control (reverse)	1.13	23.23	0.75	19.69
Control (forward)	1.14	23.15	0.76	20.06
Glass-side coating (reverse)	1.13	23.38	0.76	20.08
Glass-side coating (forward)	1.14	23.35	0.76	20.23
Double-side coating (reverse)	1.13	23.43	0.76	20.12
Double-side coating (forward)	1.14	23.39	0.76	20.27

b

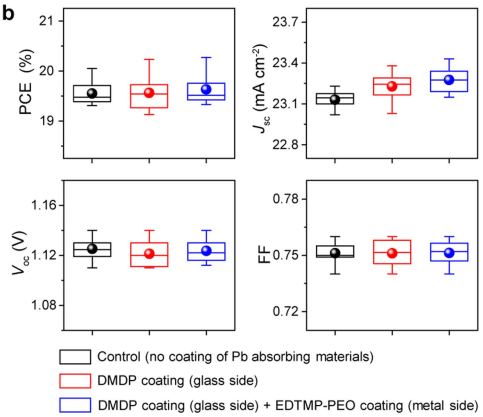

Extended Data Fig. 10 | Solar cell photovoltaic parameters. a, Detailed device photovoltaic parameters (open-circuit voltage (V_{oc}), short-circuit current density (J_{sc}), fill factor (FF) and power conversion efficiency (PCE)) from both reverse and forward J–V curves shown in Fig. 3a. **b**, Statistics of photovoltaic parameters of devices with and without the Pb-sequestering layers. Twelve devices were used for each type of device configuration. Error bars show the mean value, maximum/minimum values, and 25–75% region of data, which are represented by the circle, top/bottom bars, and rectangle, respectively.